THE ASTRONOMICAL JOURNAL VOLUME 105, NUMBER 1 JANUARY 1993

A HIGH-RESOLUTION GRAVITATIONAL LENS SURVEY

H. K. C. YEE[1]
Department of Astronomy, University of Toronto, Toronto, Ontario, M5S 1A7, Canada

ALEXEI V. FILIPPENKO[1,2]
Department of Astronomy, University of California, Berkeley, California 94720

DONGPING TANG[1,3]
Department of Astronomy, University of Toronto, Toronto, Ontario, M5S 1A7, Canada

Received 13 July 1992; revised 24 August 1992

ABSTRACT

We have conducted a search for gravitationally lensed QSOs using the Canada–France–Hawaii telescope under very good seeing conditions (median 0."70 full width at half maximum). A sample of 104 bright ($V<18.5$ mag), high redshift ($z\geqslant 1.5$) QSOs was chosen to maximize the probability of lensing. At least two r band CCD exposures were obtained of almost every QSO, with a subsequent exposure in B if there was evidence of a close neighbor. Each QSO was carefully examined by visually comparing its contour plot with that of at least one reference star from the same field. Simulations were used to determine upper limits of detectability of a close companion. Although we rediscovered some previously known systems, no definitive new cases of gravitational lensing were found. Specifically, aside from one possible exception, there are no secondary components down to 2 mag fainter than the primary at separations $\gtrsim$ 0."60, and none down to 0.5 mag fainter than the primary at separations $\gtrsim$ 0."4. These results are consistent with recent theoretical calculations of the expected distribution of separations for gravitationally lensed QSOs.

1. INTRODUCTION

Gravitationally lensed quasistellar objects (QSOs) are enormously important objects for a number of reasons; see Blandford & Narayan (1992) for a review. First, they allow us to probe the distribution of *all* matter, both luminous and dark, along different lines of sight and to different distances in the Universe. This may provide a way of directly measuring the contribution of dark matter to Ω, the cosmic density parameter. Furthermore, one can probe the distribution of matter within a lens, such as in a cluster of galaxies or a single galaxy, thereby deriving a dynamics-independent estimate of its mass. In principle, gravitational lenses can be used to deduce the value of H_0, the Hubble constant, by measurements of time delays in the variability of the separate images. Limits to the cosmological constant can also be established. Through light amplification, gravitational lensing may be influencing the derived luminosity function of QSOs and other distant objects. There is also the exciting prospect of determining the size and structure of the continuum and line-emitting regions in QSOs. In addition, the slightly different paths of the lensed components provide a valuable tool for studying the distribution of intervening absorption systems. Finally, gravitational microlensing may be used to detect, or set limits on, the presence of compact objects such as stars, brown dwarfs, or black holes; indeed, ambitious searches for massive compact halo objects in our own Galactic halo are currently in progress (Griest 1991, and references therein).

At the present time, there are about a dozen known systems with a high probability of being gravitationally lensed QSOs (Kochanek 1991a, and references therein). Some of these are particularly strong cases. For example, Q0957+561 is undeniably lensed; a cluster of galaxies ($z=0.36$) with a large dominant elliptical is seen along the line of sight to the QSO, and the VLBI jets have the same fine-scale structure except for a parity inversion, as expected. Similarly, there is much evidence for lensing of Q1115+080, Q1413+117, Q2016+112, and Q2237+031. Most of the other candidates are probably genuine lenses, but further studies are needed to be certain.

An interesting fact regarding the confirmed lenses is that the angular distance between the most widely separated images is generally large, $\Delta\theta \gtrsim 1."5$. This is in direct conflict with the theoretical expectation that galaxies and moderate clusters acting as lenses should produce small spacings, of order 1" or less. In particular, Turner *et al.* (1984) show that most lensed QSOs should have angular separations of 0."5–1."5, corresponding to that expected for single galaxy lenses. More recently, Fukugita & Turner (1991) used realistic models of galaxies to estimate that about 60% of multiply-imaged lenses should have separations $\lesssim 1."5$.

The dearth of closely-spaced QSOs among the confirmed and suspected lens candidates is generally regarded as being the result of selection effects (e.g., Turner *et al.*

[1]Guest Observer, Canada–France–Hawaii Telescope, which is operated by CNRS of France, NRC of Canada, and the University of Hawaii.
[2]Presidential Young Investigator.
[3]Present address: Department of Physics, University of Toronto, Toronto, Ontario, M5S 1A7, Canada.

1984; Burke 1986; Kochanek 1991b). Closely-spaced QSOs are difficult to identify because one needs excellent atmospheric seeing and imaging detectors having small pixel size and large dynamic range. The seeing was rarely better than 1″–1.″5 in most optical imaging studies published in the 1980s, although considerably better angular resolution was obtained in a radio snapshot survey of quasars with the Very Large Array (VLA) (e.g., Hewitt *et al.* 1987). On the other hand, most QSOs are actually radio quiet; moreover, radio structures of quasars are often larger than 1″, so confusion may arise when the splitting is small.

As noted previously, QSOs can be microlensed by stellar masses in intervening galaxies. Such lensing will alter the luminosity function of QSOs. The importance of microlensing can be indirectly inferred by studies of the statistics of foreground galaxies along the line of sight to QSOs. Microlensing events can magnify the luminosity of a QSO without producing observable image splitting. Webster *et al.* (1988a) claim to have found an excess of a factor of 3–4 in galaxy counts in the vicinity of QSOs. Similarly, Fugmann (1988) reports a substantial overabundance of galaxies in front of radio-loud quasars. Theoretically, however, such large excesses are difficult to understand (e.g., Kaiser & Tribble 1991), and other surveys have found inconclusive evidence regarding the excess of galaxies around high redshift QSOs (e.g., Magain *et al.* 1990; Crampton *et al.* 1992). Additional observations under well-controlled conditions are much desired to resolve this question.

Thus, several years ago we decided to conduct an optical search for closely-spaced, gravitationally lensed QSOs at a site with generally superior seeing conditions; see Yee *et al.* (1992). At least four other groups (Crampton *et al.* 1989; Webster *et al.* 1988b; Djorgovski & Meylan 1989; Surdej *et al.* 1988) commenced roughly contemporaneous surveys, with the latter two eventually expanding into an ESO Key Program (Swings *et al.* 1990). These extensive studies nicely complement the snapshot survey currently being conducted with the *Hubble Space Telescope* (Bahcall *et al.* 1992a; Maoz *et al.* 1993, and references therein), which has thus far identified one candidate lensed QSO (Q1208+1011) with sub-arcsecond separation (Maoz *et al.* 1992; Bahcall *et al.* 1992b; see also Magain *et al.* 1992). All the available optical data (excluding Webster *et al.* 1988b, but including the *HST* snapshots and our survey) have recently been used by Surdej *et al.* (1993) to discuss the first results on gravitational lensing statistics from a large sample (470) of QSOs.

In this paper, we present the data and preliminary results of our imaging survey of 104 high redshift QSOs, carried out at the Canada–France–Hawaii telescope (CFHT) under exceptionally good seeing conditions. Most of the data were photometrically calibrated. More detailed studies of the lensing statistics and foreground galaxy counts will be presented in future papers. In Sec. 2 we describe the sample, the observations, and the resulting data. Section 3 discusses the preliminary search for closely-spaced lens candidates. Individual interesting objects are presented in Sec. 4.

2. OBSERVATIONS AND DATA

To maximize the chance of discovering lenses, we concentrated on bright QSOs at high redshifts. The basic sample of QSOs for this program is based on all QSOs in the Hewitt & Burbidge (1987, hereafter HB87) catalog satisfying the following criteria: $z \geqslant 1.5$, $V \leqslant 18.5$ mag as listed in the catalog, $-15° < \delta < 75°$, and $|b| > 30°$. Since QSOs are found preferentially to be associated with galaxies at the same redshift (Yee & Green 1984), the high redshift criterion also ensures that there will be minimal confusion between associated and foreground galaxies in the study of excess line-of-sight galaxies. The declination criterion helps ensure the best image quality possible, and the limit on Galactic latitude minimizes confusion with foreground stars. We further place the restriction that none of the QSOs was originally discovered by searching around known galaxies. These criteria produce a heterogeneous sample of 349 QSOs, of which we observed 104.

The QSOs that we actually observed were not chosen entirely randomly. First, we restricted our observations to QSOs that had airmass less than 1.3 if possible, to improve the seeing and to minimize atmospheric dispersion (Filippenko 1982). The latter eliminates possible systematic effects that could occur when using a red star as the point spread function (PSF) reference for the blue QSO. We also normally chose the brightest available object that was within the airmass criterion. This resulted in an excess of bright QSOs being observed. Figure 1(a) illustrates the distribution of V magnitudes (as listed in HB87) of the entire sample and of the objects actually observed. Figure 1(b) shows the distribution of measured r magnitudes. Note that the r distribution has a significant tail in the faint end when compared with the V distribution. This might indicate that the V magnitudes in the literature are often overestimates. The redshift distributions of the whole sample and the observed objects are shown in Fig. 2.

The observations were performed using the direct camera at the prime focus of CFHT in three runs in 1988 and 1989. Two different CCDs were used. For the November 1988 run, the detector RCA4 was used. It is 1024×640 pixels in size with 15 μm pixel^{-1}, giving a scale of 0.″206 pixel^{-1}. This chip has a slightly uneven surface which produces significant variations in focus across the chip in the fast $f/4$ beam at the prime focus of CFHT. For the subsequent two runs in May and October 1989, we switched to a smaller but flatter chip—PHX1, a Ford Aerospace 516 ×516 pixel CCD with 20 μm pixel^{-1}, giving a scale of 0.″274 pixel^{-1}. The images from this detector are much more uniform. A detailed discussion of the image quality across the field for images from the different CCDs is given in Sec. 3.

The fields were initially imaged through a Gunn r filter (Thuan & Gunn 1976), generally with two exposures of 300 s duration each. Some fields were observed using a longer exposure to compensate for transparency problems,

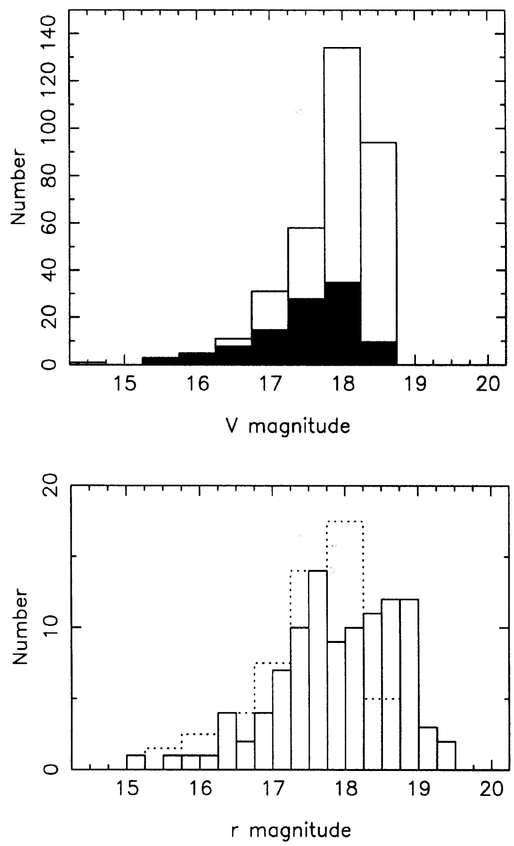

FIG. 1. Histograms of magnitude distributions of the QSO sample. The open histogram in (a) shows the distribution in V mag (from HB87) of the whole sample of 349 QSOs, while the solid histogram shows the distribution of the 104 objects actually observed. The open histogram in (b) shows the distribution of the measured r mag of the observed sample. For comparison, the V mag distribution is replotted on the same scale using a dotted line. Note the difference in shape of the two distributions, indicating that many of the V magnitudes in the literature may be overestimates.

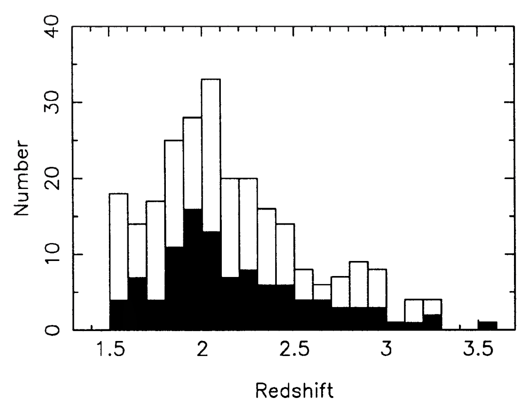

FIG. 2. Distribution of redshift of the whole sample (*open histogram*) and of the observed sample (*solid histogram*) of QSOs.

and others were observed with shorter integration to prevent saturation of the QSO images. If the object was deemed "interesting" upon real-time examination (e.g., there was a close neighbor, either stellar or resolved), a Johnson B exposure of duration 400–600 s was taken. This strategy was adopted to eliminate foreground stars projected along the line of sight as possible lens candidates; most stars do not have the same colors as QSOs. Focusing was performed often, again to ensure the highest possible image quality. In addition, typically 5–6 Gunn standard stars (Kent 1985) plus the M67 field (Schild 1983) were observed for photometric calibrations.

The data were flat fielded and bias subtracted using conventional methods. Photometry and other measurements were made with the imaging processing system PPP (Yee 1991). In Table 1, we list the properties of the objects observed with the following format: column 1, coordinate name; column 2, other names; column 3, radio emission property (R=radio-loud, O=radio-quiet); column 4, emission redshift; column 5, V mag as listed in HB87; column 6, UT date observed; columns 7 and 8, total exposure times (s) for the Gunn r and (if available) Johnson B images, respectively; column 9, measured r magnitude; column 10, signal-to-noise (S/N) ratio of the QSO r image; column 11, $B-r$ color if available; column 12, full width at half maximum (FWHM, i.e., the "seeing") of the r image PSF; column 13, absolute magnitude in the observed r band, computed using $H_0=50$ km s^{-1} Mpc^{-1} and $q_0=0$; and column 14, notes. Two QSOs at $z<1.5$ were observed serendipitously because they are in the field of higher redshift QSOs, and a few others do not satisfy at least one of our selection criteria. These are all given at the end of Table 1.

We now describe in more detail some of the items in Table 1. A uniform aperture of 5".5 diameter was used for the derivation of the r magnitudes of the QSOs. From the shape of the PSF, this diameter encompasses over 99% of the total light, given the median seeing (FWHM) of 0".70 (see below). The S/N ratio was computed using a smaller aperture of 1".4 ($\sim$2 FWHM), and is intended to provide an indication of the detectability of a very close companion object. The S/N ratio was derived from both photon statistics and uncertainties in the background sky subtraction. The measurement uncertainty for the total r magnitude is typically twice that derived from the smaller aperture. However, the total uncertainty in the r magnitude is dominated by the systematic calibration uncertainty of $\sim$0.03 mag. Many objects were observed during nonphotometric conditions; short exposures (typically 60 s) were therefore obtained of them during photometric nights for the purpose of calibration. These objects, whose calibration uncertainty is larger by a factor of $\sim$2, are indicated in column 14. Since we procured two or more images in the r band for all objects, internal photometric checks were made to ensure high photometric quality. Under photometric conditions, the r images were typically repeatable to better than 0.015 mag. Any object with a deviation of more than 0.025

TABLE 1. Journal of observations and results.

(1) Coordinate Name	(2) Other Names	(3) Type	(4) z(em)	(5) V (mag)	(6) UT Date	(7) Exp. (s) r	(8) B	(9) r (mag)	(10) S/N	(11) B − r (mag)	(12) FWHM (″ × ″)	(13) M_r (mag)	(14) Notes
0002 − 008	UM 197	O	2.18	18	10-21-89	600	—	18.61	409	—	0.92 × 0.65	−28.6	
0002 + 051	UM 18	R	1.899*	16.21	11-12-88	600	400	16.49	1358	0.37	0.90 × 0.87	−30.2	
0007 − 000	UM 208	O	2.31	17	10-22-89	300	600	18.58	424	0.13	0.72 × 0.60	−28.8	a,b
0007 + 171	4C 17.04	R	1.601+	18	11-12-88	600	400	17.60	657	0.18	0.78 × 0.69	−28.6	
0013 − 004	UM 224	O	2.09	17	10-22-89	600	600	17.79	617	0.37	0.68 × 0.64	−29.3	a
0017 + 154	3CR 9	R	2.012*	18.21	10-21-89	600	500	17.66	749	0.41	0.70 × 0.61	−29.3	
0024 + 033	UM 35	O	(2.42)	17	10-22-89	600	—	17.51	777	—	0.73 × 0.59	−30.0	a
0028 + 002	UM 252	O	1.732	18	10-22-89	660	—	18.77	414	—	0.74 × 0.63	−27.7	a,c,d
0029 + 002	UM 253	O	2.222	18	10-22-89	660	—	18.59	462	—	0.80 × 0.60	−28.7	a,c,d
0029 − 121	UM 665	O	2.65	18.0	10-22-89	600	—	18.27	533	—	0.72 × 0.67	−29.6	a
0029 + 073	—	O	3.272+	18.4	10-22-89	600	—	17.80	723	—	0.60 × 0.57	−30.8	a
0032 − 014	UM 259	O	(1.85)	17	10-21-89	600	—	18.30	508	—	0.71 × 0.66	−28.3	
0033 + 098	4C 09.01	R	1.918	17.5	11-12-88	600	—	17.94	628	—	1.26 × 1.11	−28.7	
0034 + 024	UM 52	R	(2.27)	18*	10-21-89	600	500	18.93	327	0.04	0.74 × 0.61	−28.4	
0043 + 008	UM 275	R	2.143*	17	11-12-88	600	—	18.44	310	—	1.32 × 1.28	−28.7	
0045 − 013	UM 278	R	2.53	18	10-22-89	600	—	18.48	352	—	0.58 × 0.47	−29.2	a
0046 − 067	PKS	R	2.063	18	10-22-89	600	—	17.65	761	—	0.53 × 0.52	−29.4	a
0049 + 007	UM 287	O	2.27	17.8	10-21-89	600	—	17.67	683	—	0.70 × 0.76	−29.6	
0049 + 014	UM 288	O	2.31*	17	10-21-89	600	—	17.19	906	—	0.70 × 0.67	−30.2	
0054 − 006	PKS	R	2.777+	18	10-22-89	600	—	19.36	286	—	0.52 × 0.52	−28.6	a
0055 + 004	UM 294	R	1.92	17.7	10-22-89	240	400	16.98	670	0.20	0.72 × 0.62	−29.8	a,e
0058 + 019	PHL 938	O	1.955*	17.16*	10-22-89	600	—	17.06	862	—	0.58 × 0.61	−29.8	a,f
0100 + 130	PHL 957	O	2.681*	16.57	10-22-89	500	—	16.65	1168	—	0.56 × 0.52	−31.2	a,g
0105 + 061	UM 86	O	1.96	17.2	10-21-89	600	—	17.07	688	—	0.70 × 0.66	−29.8	f
0106 + 013	4C 01.02	R	2.107	18.39	10-22-89	660	—	18.89	382	—	0.69 × 0.66	−28.2	a,d
0109 + 176	4C 17.09	R	(2.157)+	18	10-21-89	600	400	18.35	506	0.33	0.66 × 0.61	−28.8	
0114 − 089	UM 670	O	3.16	17.4	10-22-89	600	—	17.47	832	—	0.56 × 0.54	−31.0	a
0119 + 247	B2, PKS	R	2.025	18.5	10-21-89	600	—	18.40	516	—	0.59 × 0.52	−28.5	
0119 − 046	4C 04.04	R	1.948*	16.88*	10-22-89	600	—	16.90	1054	—	0.70 × 0.66	−29.9	a,h
0123 + 257	4C 25.05	R	2.358*	17.5	10-21-89	600	500	18.09	616	0.12	0.59 × 0.47	−29.4	
0132 + 205	NAB	O	1.782+	17.5*	10-21-89	600	—	17.86	701	—	0.51 × 0.46	−28.7	
0151 + 048	PHL 1222	O	1.903*	17.63	10-22-89	600	600	17.86	648	0.26	0.68 × 0.63	−28.9	a,i
0159 + 036	UM 154	O	2.44	18.2	10-22-89	600	—	17.44	800	—	0.67 × 0.58	−30.1	a
0207 − 003	UM 402	O	2.84*	17.7	10-21-89	250	400	16.96	650	0.22	0.79 × 0.58	−31.1	e
0207 + 006	UM 403	O	2.19	18*	10-22-89	600	—	18.86	358	—	0.70 × 0.61	−28.3	a
0216 + 080	—	O	2.991	18.1	10-22-89	600	—	18.13	529	—	0.82 × 0.62	−30.1	a
0226 − 038	PHL 1305	R	2.064*	16.96	10-21-89	600	—	17.41	802	—	0.81 × 0.59	−29.6	j
0229 + 131	PKS	R	2.065+	17.71	10-21-89	600	500	18.02	591	0.04	0.73 × 0.55	−29.0	
0244 − 128	PKS	R	2.201	17.1	10-22-89	600	600	18.35	482	0.20	0.72 × 0.67	−28.9	
0302 − 003	—	O	3.285	18.37	10-22-89	600	—	17.59	698	—	0.83 × 0.65	−31.0	
0348 + 061	NAB	O	2.058+	17.6	11-12-88	600	—	17.65	899	—	0.85 × 0.82	−29.3	
0406 − 127	PKS	R	1.563	18.5	10-21-89	600	900	18.54	449	0.27	0.68 × 0.48	−27.6	
0421 + 019	PKS	R	2.048*	17.04*	11-12-88	600	—	17.07	1288	—	0.80 × 0.75	−29.9	
0424 − 131	PKS	R	2.165*	17.5	11-12-88	600	—	17.70	873	—	0.74 × 0.73	−29.5	
0812 + 332	B2	R	2.420+	18	11-12-88	600	400	19.15	377	0.32	0.76 × 0.62	−28.4	
0820 + 296	OJ 234	R	2.368*	18.5	10-21-89	600	—	19.06	192	—	0.89 × 0.60	−28.4	
0836 + 195	4C 19.31	R	1.691*	17.6	11-12-88	600	—	17.62	996	—	0.73 × 0.65	−28.7	
0843 + 136	4C 13.39	R	1.875*	17.8	11-12-88	600	—	17.69	944	—	0.79 × 0.67	−29.0	
0846 + 156	—	O	2.928*	18.3	10-22-89	600	—	17.89	420	—	0.99 × 0.87	−30.3	
0903 + 175	—	O	2.756*	17.3	05-12-89	450	—	17.38	198	—	0.87 × 0.73	−30.6	k,l
0941 + 261	B2	R	2.91+	18	11-12-88	600	300	18.90	428	0.20	0.67 × 0.64	−29.3	
0955 + 472	PC	O	2.482	17.76	05-12-89	600	—	17.52	721	—	0.79 × 0.76	−30.1	m
1011 + 250	TON 490	R	1.631*	15.4*	05-12-89	330	—	16.23	998	—	0.81 × 0.81	−30.0	n
1017 + 280	TON 34	O	1.924*	15.69	05-12-89	200	—	15.11	776	—	0.84 × 0.70	−31.7	o
1123 + 264	PKS, B2	R	2.341	17.5	05-12-89	300	—	18.50	319	—	0.79 × 0.76	−28.9	p
1136 + 122	—	O	2.894*	17.6	05-12-89	900	—	18.08	622	—	0.82 × 0.76	−30.1	q
1138 + 040	PG	O	1.876	16.05	05-12-89	600	—	17.15	924	—	0.82 × 0.74	−29.5	f
1207 + 399	—	O	2.4	17.5	05-11-89	600	—	17.41	638	—	1.26 × 1.08	−30.1	
1215 + 333	GC	R	2.606+	17.5	05-11-89	600	—	17.66	767	—	1.24 × 0.98	−30.1	
1222 + 228	PG	O	2.051*	15.49	05-12-89	600	—	16.29	1424	—	0.87 × 0.86	−30.7	m,r
1225 + 317	B2	R	2.219*	15.87	05-11-89	240	—	15.76	1008	—	0.75 × 0.61	−31.5	s
1247 + 267	PG	O	2.038*	15.8	05-11-89	320	—	15.98	1418	—	0.79 × 0.74	−31.0	t
1308 + 182	4C 18.36	R	1.677*	17.5*	05-12-89	750	—	18.76	727	—	0.90 × 0.89	−27.6	l,u
1318 + 290	TON 155	O	1.703*	16.9	05-11-89	600	—	17.70	656	—	1.02 × 0.83	−28.7	c,m
1329 + 412	PG	O	1.930	16.30	05-11-89	700	—	17.43	657	—	1.12 × 1.09	−29.4	m,v

TABLE 1. (continued)

(1) Coordinate Name	(2) Other Names	(3) Type	(4) z(em)	(5) V (mag)	(6) UT Date	(7) Exp. (s) r	(8) B	(9) r (mag)	(10) S/N	(11) $B-r$ (mag)	(12) FWHM ($'' \times ''$)	(13) M_r (mag)	(14) Notes
1331+170	MC 3	R	2.081*	16.71	05-12-89	600	—	16.61	1234	—	0.94 × 0.88	−30.4	m
1358+115	—	O	2.571	16.5	05-12-89	600	—	17.33	787	—	0.94 × 0.84	−30.4	m
1413+117	—	O	2.551*	16.70	05-12-89	600	300	16.84	970	0.63	0.89 × 0.85	−30.9	w
1421+330	MKN 679	O	1.904*	16.70	05-11-89	600	—	16.49	1335	—	0.84 × 0.83	−30.2	
1442+101	OQ 172	R	3.53*	17.78	05-11-89	600	—	18.06	550	—	0.64 × 0.61	−30.8	
1517+239	LB 9612	O	1.901*	16.4	05-12-89	600	—	17.73	715	—	0.79 × 0.78	−29.0	
1548+092	—	O	2.749	17.5	05-11-89	600	—	18.81	481	—	0.77 × 0.72	−29.2	
1551+130	PKS	R	2.21+	17.65	05-11-89	600	—	18.10	550	—	0.87 × 0.73	−29.1	
1556+335	GC	R	1.646*	17	05-12-89	600	—	17.14	1000	—	0.84 × 0.82	−29.1	
1559+140	—	R	2.237	18	05-11-89	600	—	18.71	394	—	0.73 × 0.67	−28.6	
1559+173	4C 17.65	R	1.944*	17.7	05-11-89	600	—	18.59	425	—	0.80 × 0.74	−28.2	
1623+268	KP 76	O	2.49	18	05-10-89	600	—	18.80	246	—	1.13 × 1.02	−28.8	l
1623+268	KP 77	O	2.518*	16.0	05-10-89	1009	—	17.25	657	—	0.88 × 0.66	−30.4	l,x
1633+382	4C 38.41	R	1.814+	18	05-11-89	600	—	18.08	450	—	1.21 × 0.91	−28.5	
1634+176	MC 3	R	1.897*	18	05-12-89	600	300	18.91	321	0.36	0.78 × 0.77	−27.8	
1656+477	S4	R	1.622	18.0	05-12-89	600	—	17.34	631	—	0.86 × 0.77	−28.9	
1715+535	PG	O	1.920	16.30	05-11-89	400	300	16.25	1304	0.41	1.09 × 0.89	−30.5	y
2121+053	OX 036	R	1.878	17.5	05-10-89	600	—	19.31	186	—	1.16 × 0.93	−27.4	l
2134+004	PKS	R	1.936+	16.79*	11-12-88	600	—	17.26	1027	—	0.74 × 0.65	−29.5	
2134−149	—	O	2.20	18.3	10-22-89	600	—	18.90	276	—	0.76 × 0.61	−28.3	a
2150+053	4C 05.81	R	1.979	17.77	05-12-89	600	—	18.14	574	—	0.70 × 0.65	−28.7	
2158+101	4C 10.67	R	1.725	17.7	10-22-89	900	—	19.05	72	—	0.85 × 0.69	−27.4	a,y
2225−055	PHL 5200	R	1.981*	17.7	11-12-88	600	—	18.04	516	—	0.69 × 0.59	−28.8	
2227−088	PKS	R	1.561	17.5	11-12-88	600	—	17.01	1300	—	0.73 × 0.67	−29.1	
2248+192	4C 19.74	R	1.806	18.5	10-22-89	700	—	18.58	466	—	0.92 × 0.68	−28.0	a,z
2251+244	4C 24.61	R	2.328*	17.8	10-22-89	700	—	17.94	704	—	0.62 × 0.60	−29.5	a,z
2254+024	PKS	R	2.09	18	10-23-89	900	—	17.92	782	—	0.65 × 0.59	−29.1	A
2256+017	PKS	R	2.663+	18.5	10-23-89	600	—	18.72	396	—	0.70 × 0.57	−29.1	
2303+183	—	R	1.557	18	10-22-89	700	—	18.49	531	—	0.63 × 0.62	−27.6	a,z
2320+079	PKS	R	2.09	17.5	11-12-88	600	—	18.65	445	—	0.75 × 0.73	−28.4	
2333+019	PB 5468	R	1.871	18	10-23-89	600	400	18.64	378	0.05	0.94 × 0.80	−28.0	
2345+003	UM 180	O	1.96	17.7	11-12-88	300	—	18.38	430	—	0.87 × 0.81	−28.5	B
2345+061	4C 06.76	R	1.546	17.5	10-22-89	600	500	17.93	643	0.37	0.68 × 0.65	−28.1	a
2348−011	UM 184	O	3.01*	18.0	10-21-89	600	500	18.64	415	1.02	0.70 × 0.53	−29.6	
2353+154	PKS	R	1.801	18	10-21-89	600	—	18.11	594	—	0.79 × 0.60	−28.5	
2354+144	PKS	R	1.81	18.18*	10-21-89	600	400	18.64	432	0.07	0.70 × 0.53	−27.9	
2355−106	PKS	R	1.626	17.7	11-12-88	600	500	18.95	279	0.27	1.08 × 1.05	−27.3	
2356+016	UM 193	O	(2.13)	18	10-23-89	600	300	18.36	471	0.29	0.88 × 0.73	−28.7	
2359−022	UM 196	O	2.82*	18	10-22-89	660	—	18.77	392	—	0.69 × 0.66	−29.3	a,c,d
0120+026	UM 100	R	—	18	10-21-89	840	600	17.01	—	1.95	0.79 × 0.62	—	C,D,E
0256−000	—	O	3.367	18.72	10-21-89	550	—	17.45	768	—	0.74 × 0.54	−31.2	C,F
0846+513	W1	O	1.86	17*	10-22-89	600	400	19.46	154	0.64	0.90 × 0.73	−27.2	C
1318+290	TON 156	O	0.549	16.4*	05-11-89	600	—	16.67	886	—	0.98 × 0.76	−26.4	C,c,m
2359−022	UM 195	O	0.86	18.9	10-22-89	660	—	18.71	417	—	0.69 × 0.66	−25.6	C,a,c,d

Explanation of Columns.

(1) Coordinate name. (2) Other names. (3) Radio emission property (R = radio-loud, O = radio-quiet). (4) Emission redshift, from HB87. Uncertain redshifts are given in parentheses. A plus sign indicates that absorption has been seen but no redshift systems have been measured. An asterisk indicates that absorption redshifts have been reported. (5) V magnitude listed in HB87. An asterisk indicates the object is known to be variable. (6) UT date observed. (7) Total exposure time for Gunn r images. (8) Total exposure time for Johnson B images. (9) Measured r magnitude. (10) S/N ratio of QSO r image. (11) $B-r$ color. (12) FWHM of r image PSF, long axis by short axis. (13) Absolute magnitude in observed r band, computed with $H_0 = 50$ km s^{-1} Mpc^{-1} and $q_0 = 0$. (14) Notes to TABLE 1:

a: Calibrated using 60 s r exposure obtained on 10-23-89 UT.
c: Two quasars in the same CCD field.
e: 1 r exposure, 300 s, was saturated; not used.
g: 5 r exposures, 100 s each.
i: Meylan et al. (1990) double QSO.
k: 2 r exposures: 1 for 200 s, 1 for 250 s.
m: Non-photometric conditions; r approximate (±0.1 mag).
o: 4 r exposures, 50 s each. 1 r exposure, 100 s, saturated; not used.
q: 3 r exposures, 300 s each.
r: 3 r exposures, 200 s each.
t: 4 r exposures, 80 s each. 1 r exposure, 100 s, saturated; not used.
v: 3 r exposures: 2 for 300 s each, 1 for 100 s.
x: 5 r exposures: 3 for 150 s each, 1 for 259 s, 1 for 300 s.
z: 2 r exposures, 350 s each.
B: 1 r exposure, 300 s. Other 300 s exposure failed: bad tracking.
D: Not a quasar — low-z galaxy.
F: 2 r exposures: 1 for 250 s, 1 for 300 s.

b: Other 300 s exposure failed: bad focus.
d: 2 r exposures, 330 s each.
f: 4 r exposures, 150 s each.
h: 4 r exposures: 3 for 160 s each, 1 for 120 s.
j: 3 r exposures: two for 150 s each, one for 300 s.
l: Non-photometric conditions; r approximate ($\pm \gtrsim 0.3$ mag).
n: 2 r exposures: 1 for 150 s, 1 for 180 s.
p: 1 r exposure. Also, did on 05-11-89 UT for 900 s (3 r exposures, 300 s each): $S/N = 428$, $r = 18.49$ mag, FWHM = $0.91'' \times 0.82''$.
s: 3 r exposures, 80 s each. 1 r exposure, 100 s, saturated; not used.
u: 3 r exposures, 250 s each.
w: Magain et al. (1988) lens. Magnitudes are sum of 4 components.
y: 2 r exposures: 400 s, 500 s. (For PG 1715+535: 200 s each.)
A: 3 r exposures, 300 s each; 1 has satellite trail.
C: Observed, but not in sample.
E: 6 r exposures: 4 for 60 s each, 2 for 300 s each. 3 B exposures: 2 for 150 s each, 1 for 300 s. 3 Gunn i exposures, 150 s each.

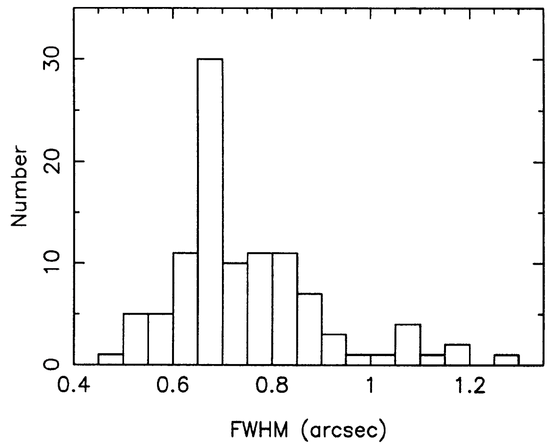

FIG. 3. Distribution of FWHM (seeing) of r images of observed QSOs.

mag between two successive r frames was deemed nonphotometric.

The FWHM was estimated using the width of the half-power contour of the contour map of either the QSO or a star of similar brightness in the field. The object was sinc-shifted to have an integer pixel centroid before making the contour plot, and the half-power contour was defined as the contour which has $\frac{1}{2}$ the value of the peak pixel. Most of the images give a slightly noncircular PSF. The FWHMs are listed as the long axis diameter times the short axis diameter. In almost all cases, the long axis points SE to NW. To obtain a relatively uniform data set, program objects were observed (with few exceptions) only when the seeing conditions were judged to be $\lesssim 1''$. The distribution of the FWHM of the images (after averaging the long and short axis FWHMs) is plotted in Fig. 3. A median seeing of $\sim 0\farcs70$ is obtained for the whole sample. The data from the October 1989 run were of particularly high quality, with a median seeing of $\sim 0\farcs65$.

3. THE SEARCH FOR LENS CANDIDATES

3.1 Large-Separation Candidates

With typical seeing of $0\farcs70$, large-separation lens candidates that are more than $1\farcs5$ from the QSO can be readily detected visually. In Table 2 we list all objects with stellar profiles that are brighter than $r=23.5$ mag and within $10''$ radius from the QSO. The following format is used: column 1, QSO name; column 2, radial distance of the companion from the QSO; column 3, r magnitude of the companion; column 4, $B-r$ color of the companion; column 5, $B-r$ color of the QSO for comparison; and column 6, notes. Additional comments on some objects can be found in Sec. 4.

The $10''$ distance criterion is very conservative; the lens candidate having the largest separation in past searches is about $6''$, and most have separations of only $1''$–$3''$ (see list in Blandford & Narayan 1992). Given that the separation of lensed images should be on the order of a few arcseconds for a galaxy cluster potential, it is unlikely that objects with separations larger than $\sim 7''$ are good candidates.

TABLE 2. List of close stellar companions.

(1) QSO Name	(2) Distance ($''$)	(3) r (mag)	(4) $B-r$ (mag)	(5) $(B-r)_{\rm QSO}$ (mag)	(6) Notes
0007+171	8.3	20.93	1.60	0.18	Confirmed star
0013−004	3.2	23.2	0.8	0.37	
0034+024	9.9	19.10	0.69	0.04	
0106+013	7.0	21.62	—	—	
0119−046	7.9	22.08	—	—	
0123+257	7.5	19.47	0.86	0.12	
0151+048	3.3	21.66	0.13	0.26	Binary QSO
	6.7	22.51	>1.5	0.26	
0229+131	6.7	20.26	1.23	0.04	
0812+332	6.3	18.30	1.88	0.32	
0941+261	4.4	18.59	0.52	0.20	Confirmed star
1559+140	8.4	21.16	—	—	
1715+535	3.6	16.19	0.68	0.41	Confirmed star
2333+019	6.8	21.64	~2.0	0.05	
2345+061	5.7	20.94	2.22	0.37	

We can also use a photometric color comparison to rule out most of the large-separation candidates. Note that we have not measured $B-r$ colors for all companions; however, the three objects without colors are all more than $7''$ away from the QSO. Lensed QSO components can be of different colors due to differential extinction of one or more components through the lensing galaxy, or due to intrinsic QSO variability coupled with unequal time delays for the components. A prime example of the former case is Q2237+031 (Yee 1988; Nadeau *et al.* 1991); the maximum difference in $B-r$ is about 0.25 mag (see the photometry in Corrigan *et al.* 1991). Based on this, we choose $(B-r)_{\rm companion}-(B-r)_{\rm QSO}<0.35$ mag as the criterion for accepting a stellar companion as a bona fide lens candidate. These potentially interesting objects were observed spectroscopically using the 3 m Shane reflector at Lick Observatory; we discuss them in more detail in Sec. 4. Of course, it is possible for larger differential reddening or variability to occur, and we can be certain that no lens is missed only if spectra are available for all stellar companions. We plan to obtain spectra of the best candidates in Table 2 with the Shane reflector at Lick Observatory.

In the sample of 104 QSOs, no new large-separation lenses were found. We rediscovered the clover-leaf lens (Q1413+117; Magain *et al.* 1988), and the double QSO PHL 1222 (Q0151+048) of Meylan *et al.* (1990). These objects were chosen to be observed randomly without real-time cognizance of their special status. Two other QSOs (Q0941+261 and Q1715+535) have relatively close companions ($<5''$ separation) with color differences of less than 0.35 mag. These were spectroscopically confirmed to be stars. Fifty-two of our objects were also observed as part of the *HST* snapshot survey (Bahcall *et al.* 1992a; Maoz *et al.* 1993, and references therein); in all cases (possibly except PKS 2251+244; see Sec. 4), the results are consistent with ours.

3.2 The Search for Small-Separation Lenses

In the following, we describe our method of a preliminary search for close-separation lenses ($\Delta\theta \lesssim 1''$) using visual comparison of the contour plot of a QSO image and reference stars from the same field. To create a contour plot of the QSO or a reference star, we first shift the object image iteratively using a sinc function interpolator until the object's peak pixel is centered on an integer pixel position; see Yee & Green (1987) for a more detailed description. A logarithmic contour plot is then made with successive contours being $\frac{1}{4}$ or $\frac{1}{2}$ the value of the previous contour, using the peak pixel as the starting point. Contour plots made in exactly the same manner are created from all other sufficiently bright stars in the field to be used for comparison. Usually one to three stars can be chosen. The QSO contour map is then compared by eye by matching it onto the reference star contour map to search for distortions that may be caused by one or more small-separation lens candidates. Typical examples of QSO and reference star images are shown in Fig. 4.

An important factor that affects the confidence of the detection of a close companion is the uniformity of the PSF shape over the CCD field. We map the distortion of the PSF as a function of position on the two CCD fields by observing star clusters. Contour maps of relatively isolated stars chosen from different parts of the field are compared using the method described above. For the RCA4 images, large variations in the PSF shape are found. Typically the FWHM varies about 5%–10% across the central $\frac{3}{4}$ of the chip, and differences as large as 20% are seen in some areas near the corners. The bulk of the data were taken with the PHX1 chip which has a much flatter surface. Here, the PSF shape across most of the chip stays constant, with the exception of a $40'' \times 25''$ area at the NE corner of the field where the FWHM of the images are typical 5% shorter along the NS axis. The variation of PSF causes us to be more conservative in picking out possible candidates. However, since more than one reference star can be chosen for comparison with the QSO in an overwhelming majority of cases, we are able to eliminate most false detections due to intrinsic variations in the PSF.

Close examination of all QSO images in the prescribed method reveals no candidates with a definitive close companion. Simulations are used to determine the upper limit of detectability of a close companion. There are two parameters to explore in the simulation: the separation, $\Delta\theta$, and the magnitude difference, Δm, between the QSO and the companion. To first order, we can assume that images taken under different seeing conditions have PSF shapes that scale spatially with the FWHM, thereby allowing us to explore the separation parameter in terms of the FWHM. Although the simulations are made with only one lensed component, the limits obtained are applicable to multicomponent lens systems having the largest separation corresponding to the simulated two-component separation. The simulations are performed using the program PPP, and consist of artificially adding scaled PSFs (determined from the same frame) with various values of $\Delta\theta$ and Δm to a real QSO image in order to assess the limits at which a close companion is detectable. This allows one to set detectability limits on the $\Delta\theta$–Δm plane for QSO images of a given S/N ratio. Typical simulations are shown in Fig. 5. Simulations were performed for QSOs with various S/N ratios and the estimated detection limits are listed in Table 3. The typical confidence in the limits is about $\pm 10\%$–15%. Note that the limiting separation is a strong function of Δm, but not the S/N ratio (as long as it is high), of the QSO image. Any objects separated from the QSO by more than ~ 2 FWHM can easily be detected to the completeness limit of $r \approx 23.5$ mag. Thus, based on the typical seeing and S/N ratio of the survey, we conclude that we detect no definitive lens candidates down to 2 mag fainter than the primary at separations greater than $\sim 0\farcs60$, and no candidates down to 0.5 mag fainter than the primary at separations greater than $\sim 0\farcs4$. One possible candidate (Ton 34) is described in Sec. 4.

Although this method is simple and effective in detecting close companions, the limits that we set are relatively conservative, partly due to the variation in focus across the field and partly due to the fact that the detection is performed by eye. Our separation limits are typically a factor of 1.5 larger than those of Crampton *et al.* (1992) who used the method of PSF subtraction. A study to improve on the detection limits using similar methods is underway and will be reported in a future paper. Note that although PSF subtraction can determine to a high precision whether the QSO image matches a PSF, it usually is not able to recover exactly the flux or the shape of the artificially created component if the separation is too small. For example, performing a PSF subtraction of a simulation with a $\Delta m = 0.5$ mag companion added at a distance of 0.25 FWHM from the primary, the residual component has $\Delta m \approx 3.5$ mag.

The small number of objects in our sample permits us only to set limits in comparisons with theoretical calculations of the expected distribution of separations for lensed QSOs. Furthermore, no current calculation has taken into account the distribution of magnitude differences between the lensed components. Using more realistic models of galaxies than those of Turner *et al.* (1984), Fukugita & Turner (1991) derived the probability function of angular separation. They estimated that about 60% of multiply-imaged lenses have separation less than $1\farcs5$. Given that there are ~ 10 widely spaced lens systems out of the ~ 4000 QSOs in HB87, and ignoring amplification bias, the nondetection of sub-arcsecond lenses in our sample is consistent with their calculation. A more detailed study of the frequency of gravitational lensing, combining several survey samples including the present one, is given by Surdej *et al.* (1993).

4. NOTES ON INDIVIDUAL OBJECTS

(1) *Q0007+171 (4C 17.04)*. A companion $8\farcs3$ from the QSO has $r = 20.93$ mag and $B - r = 1.6$ mag. Also, there is a much redder companion $10\farcs5$ from the QSO, with $r = 22.53$ mag and $B - r = 3.2$ mag. Spectra of the QSO and its closest neighbor were obtained simultaneously on 12-14-88 UT with a long-slit CCD spectrograph (position angle 185°) on the 3 m Shane reflector at Lick Observatory, and it was clear that the companion is a star. No spectra

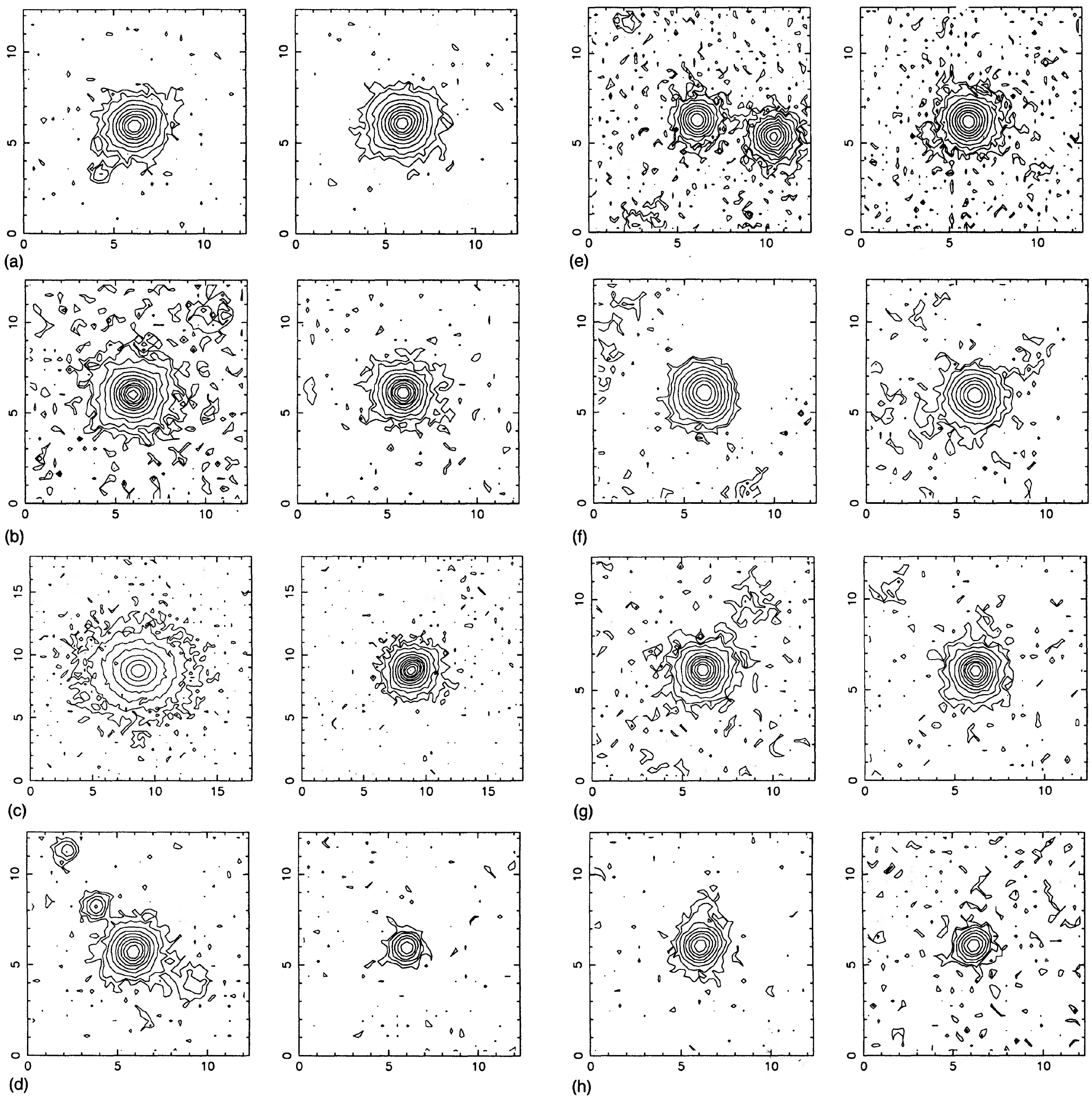

FIG. 4. Contour plots of selected QSO images. The scales marked are in arcseconds, with North to the top and East to the left. Contours are factors of 2 apart starting from the peak pixel value of the object. A reference star (PSF) contour map is shown to the right. Note that it does not have numerically the same contour levels as the QSO map; instead, the contours start from *its* own peak pixel value. (a) Q0013−004 (UM 224). The companion object is probably a star, being significantly redder than the QSO. (b) Q0100+130 (PHL 957). (c) Q0120+026 (UM 100). The image clearly shows a large galaxy. This may be a misidentification in the original survey. (d) Q0151+048 (PHL 1222). The nearest stellar object to the NE is the companion QSO; this is the binary QSO of Meylan *et al.* (1990). A third stellar object is farther to the NE. The object to the SW is a galaxy with $r=22.35$ mag. (e) B2 0941+261. The QSO is to the E. The western object is slightly redder than the QSO and is not a lens candidate. (Note that the companion object is on a bad column, causing slight distortions in the contours.) (f) Q1017+280 (Ton 34). The QSO shows slightly broader contours at the center. A residual is found upon PSF subtraction. (g) PKS 2251+244. A small residual is found for this QSO upon PSF subtraction, but no companion is seen in the *HST* images of Maoz *et al.* (1993b). (h) PKS 2256+017. This QSO shows a faint asymmetric fuzz component which is likely to be an intervening galaxy.

were obtained of the redder object, since its color differs substantially from that of the QSO.

(2) *Q0013-004 (UM 224)*, Fig. 4(a). Our r image confirms the uncertain classification of Crampton *et al.* (1992) that the close companion 3".2 SE of the QSO is stellar in shape. The object has $r=23.2$ mag and $B-r\approx0.8$ mag. This is ~0.4 mag redder than the QSO; hence, it is not considered to be a very good lens candidate. However, given the small separation, the relatively similar $B-r$ colors, and the uncertain photometry for the faint component, this object merits spectroscopic study.

(3) *Q0100+130 (PHL 957)*, Fig. 4(b). Crampton *et al.*

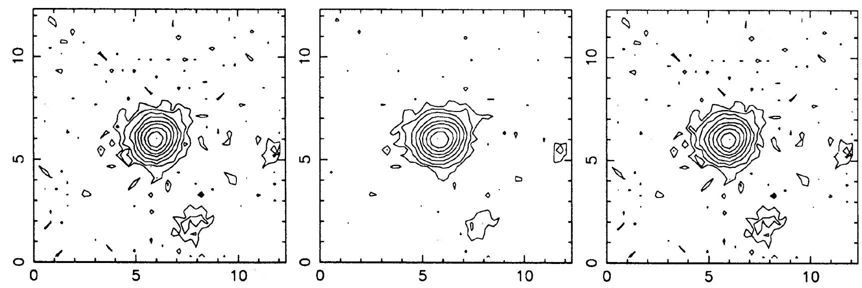

FIG. 5. Examples of simulations for determining detection limits. The contours are defined the same way as in Fig. 4. Q0244−128 is shown in the first panel. This is an image from one 300 s exposure with a FWHM of 2.57 pixels (0″7) and a S/N ratio of 340 in the central 2 FWHMs. In the second panel a companion 0.5 FWHM to the east and 0.5 mag fainter than the QSO has been added. The third panel shows the result when a companion 1.0 FWHM to the east and 3.5 mag fainter is added.

(1992) reported that this is a possible close-pair candidate. A residual was found by them when they subtracted the PSF from two different stars. However, they also commented that this could be due to artifacts in the data. Using the PSF subtraction routine in PPP (Yee & Green 1987), we found no residual in the QSO image after subtracting a PSF created using the star south of the QSO, which is 0.9 mag fainter than the QSO itself.

(4) *Q0120+026 (UM 100)*, Fig. 4(c). MacAlpine *et al.* (1977) listed this object as a possible QSO with a broad feature at 5200 Å. Fairall (1978) identified features at 5195 and 5300 Å as Lyα and N V λ1240 at $z=3.272$. However, our images show a bright, red galaxy at the position of the object with no obvious blue nuclear component ($r=17.01$ mag, $B-r=1.95$ mag). The color is indicative of a low redshift, early-type galaxy. A spectrum of Q0120+026, obtained on 11-08-89 UT with the 3 m Shane reflector at Lick Observatory, confirms this classification. There are several possible explanations for these observations. Most likely, this is simply a misidentification of a galaxy as a QSO. However, it is interesting that such a red object was found in the UM survey. Perhaps this is a highly variable active object that happened to be in a quiescent state when we observed it. Alternatively, it might be a faint QSO that was being microlensed (and hence amplified) by stars in the large red galaxy at the time of the discovery observations.

(5) *Q0151+048 (PHL 1222)*, Fig. 4(d). This is the binary QSO found by Meylan *et al.* (1990). Our photometry shows the second component at 3″3 NE with $r=21.66$ mag and $B-r=0.13$ mag. The primary QSO has $B-r=0.26$ mag. A third stellar image is 6″7 away with $r=22.51$ mag and is not detected in the B image. On 11-08-89 and 12-01-89 UT we obtained spectra of this third object with the 3 m Shane reflector at Lick Observatory, but the results were inconclusive. The object SW of the QSO is a galaxy.

(6) *Q0846+513*. This QSO is known to be a close neighbor to a bright galaxy. We chose to observe it in morning twilight knowing this fact (from the finder chart), and hence it is not included in the sample. Our images show no signs of it being macrolensed, consistent with the results of Maoz *et al.* (1993).

(7) *B2 0941+261*, Fig. 4(e). A bright, blue stellar object ($r=18.59$ mag, $B-r=0.52$ mag) is 4″4 to the west of the QSO. The QSO has $r=18.90$ mag, $B-r=0.20$ mag. Spectra of the QSO and its companion were obtained simultaneously on 12-14-88 UT with a long-slit CCD spectrograph (position angle 262°) on the 3 m Shane reflector at Lick Observatory. The blue object is not a QSO (see also Wills & Wills 1976). The other nearby objects in the field are galaxies.

(8) *Q1017+280 (Ton 34)*, Fig. 4(f). The QSO is the NW stellar object in a bright pair with 15″5 separation. This is the brightest QSO in our sample. The contour plot of the QSO shows a slight broadening in the center. PSF subtraction leaves a residual 3.4 mag fainter than the primary. This is our most probable close-pair candidate; the proximity of the reference PSF star to the QSO should make focus variations minimal. However, given that the PSF star is 0.8 mag fainter than the QSO, and that this field did not flatten particularly well, a small nonlinearity may cause the result. Further observations with higher S/N ratio and finer angular resolution will be needed for a definitive identification.

(9) *Q1623+268 (KP77)*. Crampton *et al.* (1992) listed this as a possible close pair. Our PSF subtraction serves as an illustration regarding the uncertainty in the positive detection of very close pairs. We have several images of this field with different integration times. With the two 300 s integration images, we used two stars which are 1.2 and 1.6 mag fainter than the QSO (SSE and NEE of the QSO, respectively). Both of these PSFs resulted in a faint resid-

TABLE 3. Close pair detection limits.[a]

Δm (mag) =	0.5	2.0	3.5	5.0
$S/N=1000$	0.40	0.55	0.85	1.70
$S/N=700$	0.45	0.65	0.95	1.75
$S/N=350$	0.45	0.70	1.00	1.75

[a]Separation $\Delta\theta$ in FWHM of stellar PSF.

ual, centered almost on the QSO itself. With the two 150 s exposures, we were able to use the two bright stars N of the QSO ($\sim$0.9 mag brighter than the QSO) which were saturated in the longer exposure frames. With these two stars, the PSF subtraction left no residuals. Similarly, using the two fainter stars, no residual was found. The reason for these inconsistent results is not clear. One possibility is that there is a slight nonlinearity in the 300 s QSO images. However, based on the second result, we conclude that there is no close companion to this QSO.

(10) *PG 1715+535*. The bright stellar object 3".6 SW of the QSO (position angle 258°) is a star with different color from that of the QSO. ($B-r$=0.68 and 0.41 mag for the star and the QSO, respectively.) Spectra of both objects, obtained simultaneously on 06-02-89 UT with a long-slit CCD spectrograph on the 3 m Shane reflector at Lick Observatory, confirm this result. Crampton *et al.* (1992) reported that Arnaud (1990) reached the same conclusion spectroscopically.

(11) *PKS 2134+004*. Crampton *et al.* (1992) listed this as a possible close pair. We performed a PSF subtraction using a star NW of the QSO and 0.7 mag fainter. No residual was found.

(12) *PKS 2251+244*, Fig. 4(g). Crampton *et al.* (1989) found a residual upon subtracting a PSF. Subsequently, Crampton *et al.* (1992) reported that further observations did not confirm the residual. However, from our images, PSF subtraction using two different stars also leaves a residual of $r \approx 21.2$ mag ($\Delta m \approx 3.3$ mag). Subtracting the two stars from each other leaves no residual. Thus, it appears that this QSO suffers an inconsistency in PSF subtraction similar to that of Q1623+268 (KP77). The matter appears to have been settled by the recent *HST* image of PKS 2251+244 (Maoz *et al.* 1993), which shows no evidence for a companion.

(13) *PKS 2256+017*, Fig. 4(h). This QSO shows a definite asymmetrical fuzzy component to the N. PSF subtraction indicates that this is a close intervening galaxy almost along the line of sight to the QSO ($\sim$1".5 away). The magnitude of the galaxy is $r \approx 24$ mag.

The authors would like to thank the staff and the time allocation committee of the CFHT for their assistance at the telescope and support of this project, respectively. H.K.C.Y. acknowledges the support of the Natural Science and Engineering Research Council of Canada in the form of an operating grant and a University Research Fellowship. A.V.F. is grateful for the financial assistance of the National Science Foundation under Grant No. AST-8957063.

REFERENCES

Arnaud, J. 1990, private communication
Bahcall, J. N., Maoz, D., Doxsey, R., Schneider, D. P., Lahav, O., & Yanny, B. 1992a, ApJ, 387, 56
Bahcall, J. N., Maoz, D., Schneider, D. P., Yanny, B., & Doxsey, R. 1992b, ApJ, 392, L1
Blandford, R. D., & Narayan, R. 1992, ARA&A (in press)
Burke, B. 1986, in Quasars, edited by G. Swarup and V. Kapahi (Reidel, Dordrecht), p. 517
Corrigan, R. T., *et al.* 1991, AJ, 102, 34
Crampton, D., McClure, R. D., & Fletcher, J. M. 1992, ApJ, 392, 23
Crampton, D., McClure, R. D., Fletcher, J. M., & Hutchings, J. B. 1989, AJ, 98, 1188
Djorgovski, S., & Meylan, G. 1989, in Gravitational Lenses, edited by J. M. Moran, J. N. Hewitt, and K.-Y. Lo (Springer, Berlin), p. 173
Fairall, A. P. 1978, MNAS So. Africa, 37, 41
Filippenko, A. V. 1982, PASP, 94, 715
Fugmann, W. 1988, AA, 204, 73
Fukugita, M., & Turner, E. L. 1991, MNRAS, 253, 99
Griest, K. 1991, ApJ, 366, 412
Hewitt, A., & Burbidge, G. 1987, ApJS, 63, 1 (HB87)
Hewitt, J. N., Turner, E. L., Burke, B. F., Lawrence, C. R., Bennett, C. L., Langston, G. I., & Gunn, J. E. in Observational Cosmology, edited by A. Hewitt, G. Burbidge, and L. Z. Fang (Reidel, Dordrecht), p. 747
Kaiser, N., & Tribble, P. 1991, in The Space Distribution of Quasars, edited by D. Crampton, ASP Conf. Series, 21, 304
Kent, S. M. 1985, PASP, 97, 165
Kochanek, C. S. 1991a, ApJ, 373, 354
Kochanek, C. S. 1991b, ApJ, 379, 517
MacAlpine, G. M., Smith, S. B., & Lewis, D. W. 1977, ApJS, 34, 95
Magain, P., Remy, M., Surdej, J., & Swings, J.-P. 1990, in Gravitational Lensing, edited by Y. Mellier *et al.* (Springer, Berlin), p. 88
Magain, P., Surdej, J., Swings, J.-P., Borgeest, U., Kayser, R., Kühr, H., Refsdal, S., & Remy, M. 1988, Nature, 334, 325
Magain, P., Surdej, J., Vanderriest, C., Pirenne, B., & Hutsemékers, D. 1992, A&A (in press)
Maoz, D., Bahcall, J. N., Doxsey, R., Schneider, D. P., Bahcall, N. A., Lahav, O., & Yanny, B. 1993, ApJ (in press)
Maoz, D., *et al.* 1992, ApJ, 386, L1
Meylan, G., Djorgovski, S., Weir, N., & Shaver, P. 1990, in Gravitational Lensing, edited by Y. Mellier *et al.* (Springer, Berlin), p. 111
Nadeau, D., Yee, H. K. C., Forrest, W. J., Garnett, J. D., Ninkov, Z., & Pipher, J. L. 1991, ApJ, 376, 430
Schild, R. E. 1983, PASP, 95, 1021
Surdej, J., *et al.* 1993, AJ (submitted)
Surdej, J., *et al.* 1988, in Proceedings of a Workshop on Optical Surveys for Quasars, edited by P. S. Osmer, A. C. Porter, R. F. Green, and C. B. Foltz (Astr. Soc. Pac., San Francisco), p. 183
Swings, J.-P., Magain, P., Remy, M., Surdej, J., Smette, A., Hutsemékers, D., & Van Drom, E. 1990, in Gravitational Lensing, edited by Y. Mellier *et al.* (Springer, Berlin), p. 83
Thuan, T. X., & Gunn, J. E. 1976, PASP, 88, 543
Turner, E. L., Ostriker, J. P., & Gott, J. R. 1984, ApJ, 284, 1
Webster, R. L., Hewett, P. C., Harding, M. E., & Wegner, G. A. 1988a, Nature, 336, 358
Webster, R. L., Hewett, P. C., & Irwin, M. J. 1988b, AJ, 95, 19
Wills, D., & Wills, B. J. 1976, ApJS, 31, 143
Yee, H. K. C. 1988, AJ, 95, 1331
Yee, H. K. C. 1991, PASP, 103, 396
Yee, H. K. C., Filippenko, A. V., & Tang, D. 1992, in Gravitational Lenses (Proceedings of the Hamburg Conference) (in press)
Yee, H. K. C., & Green, R. F. 1984, ApJ, 280, 79
Yee, H. K. C., & Green, R. F. 1987, AJ, 94, 618